NASA Technical Memorandum 106163
AIAA–93–3389
ICOMP–93–16

Grid Adaptation Using Chimera Composite Overlapping Meshes

Kai-Hsiung Kao
Institute for Computational Mechanics in Propulsion
Lewis Research Center
Cleveland, Ohio

Meng-Sing Liou
Lewis Research Center
Cleveland, Ohio

and

Chuen-Yen Chow
University of Colorado
Boulder, Colorado

(NASA-TM-106163) GRID ADAPTION
USING CHIMERA COMPOSITE OVERLAPPING
MESHES (NASA) 34 p

N93-27065

Unclas

G3/64 0167916

NASA

Grid Adaptation Using Chimera Composite Overlapping Meshes

Kai-Hsiung Kao
Institute for Computational Mechanics in Propulsion
NASA Lewis Research Center
Cleveland, OH 44135

Meng-Sing Liou
NASA Lewis Research Center
Cleveland, OH 44135

and

Chuen-Yen Chow
Department of Aerospace Engineering Sciences
University of Colorado
Boulder, CO 80309

ABSTRACT

The objective of this paper is to perform grid adaptation using composite overlapping meshes in regions of large gradient to capture the salient features accurately during computation. The Chimera grid scheme[1], a multiple overset mesh technique, is used in combination with a Navier-Stokes solver. The numerical solution is first converged to a steady state based on an initial coarse mesh. Solution-adaptive enhancement is then performed by using a secondary fine grid system which oversets on top of the base grid in the high-gradient region, but without requiring the mesh boundaries to join in any special way. Communications through boundary interfaces between those separated grids are carried out using tri-linear interpolation. Applications to the Euler equations for shock reflections and to a shock wave/boundary layer interaction problem are tested. With the present method, the salient features are well resolved.

1

1. INTRODUCTION

During the last decade both structured and unstructured grid systems have been developed and applied for the computations in various CFD problems. It is well known that the accuracy of the computational solutions to analytical equations is strongly influenced by the discretization of the space in which a solution is sought. In general, the introduction of a highly dense distribution of points throughout a computational domain will yield a more accurate answer than a coarse distribution. However, limitations in computer processing speed and accessible memory prohibit such a scenario. An appropriate alternative, for example a grid adaptation method, would be to improve the accuracy of the computation where needed.

Many different solution-adaptive techniques have been developed and implemented. Gnoffo[2] modelled the mesh as a network of springs whose constants were determined from flow field gradients. Brackbill[3] and Saltzman and Brackbill[4] used variational methods. Berger[5] had developed an adaptive refinement method which dynamically embedded finer and finer grids to resolve flow gradients. Eiseman[6,7] developed the method of mean value relaxation and reviewed existing adaption concepts. Other adaption methods are based upon equidistribution techniques; Nakahashi and Deiwert[8] used a spring-torsion analogy to adapt the grid and Connett et al.[9,10] based their algorithm on the method of minimal moments.

Many works have been devoted to developing techniques and methods that address two major problem areas in grid generation. They are (1) the large amount of time required to generate a grid for a complex domain, and (2) the ability to generate a grid that meets the users quality requirements (e.g., smoothness, clustering, orthogonality). Unfortunately, grid adaptation techniques usually created high aspect-ratio or highly skewed cells to align with the high-gradient features, resulting in a reduced convergent history.

A general motivation of the present study is to develop a grid adaptation

method that not only enhances the accuracy of solutions by using fine grid in high-gradient regions, but is also capable of handling complex geometries with cells of minimal skewedness. The present methodology uses the Chimera composite overlapping mesh system to improve geometric flexibility, and to achieve grid adaptation efficiently. It is proposed that composite grid schemes use two or more simple meshes to map complex configurations. The use of a multiple grid approach can yield better grid resolution, simplify the application of boundary conditions, and ease the task of grid generation. Because the overset meshes are independent of each other and the global mesh, they can readily be embedded in arbitrary orientation with respect to the global grid. This approach has the following two merits. First, it gives geometrical independence between grids. Second, it allows natural alignment and clustering of grids with interesting features in the solution.

In the following sections, we describe the governing equations, basic solver algorithm, and the solution-adaptative enhancement method using Chimera overlapping meshes. Applications are presented for the shock reflection, 15° ramp channel, flat plate boundary layer and shock wave/boundary layer interaction problems.

2. GOVERNING EQUATIONS

The Navier-Stokes equations can be expressed in an integral form in a volume v with enclosing surface s as follow:

$$\int_v \frac{\partial \mathbf{U}}{\partial t} dv + \oint_s \vec{n} ds \cdot (\mathbf{F} - \mathbf{F}_v) = 0, \tag{1}$$

where the conservative variable $\mathbf{U}$ is:

$$\mathbf{U} = [\rho, \rho\vec{u}, \rho E]^T,$$

the inviscid flux $\mathbf{F}$:

$$\mathbf{F} = [\rho\vec{u}, \rho\vec{u}\vec{u} + p\tilde{I}, \rho H \vec{u}]^T,$$

3

the viscous flux $\mathbf{F}_v$:

$$\mathbf{F}_v = [0, \tilde{\tau}, \tilde{\tau}\vec{u} + \vec{q}]^T,$$

and the equation of state for ideal gas:

$$p = (\gamma - 1)\rho e \qquad (2)$$

Here e represents the internal energy. The vector quantities, expressed in terms of Cartesian coordinates, are denoted with an overhead arrow $(\vec{\ })$, and the tensor with an overhead tilde $(\tilde{\ })$ or a dyadic notation such as $\vec{u}\vec{u}$.

Assuming a Newtonian fluid and using Stoke's hypothesis, the stress tensor $\tilde{\tau}$ and the heat flux vector $\vec{q}$ are expressed in terms of gradient (∇) of relevant quantities:

$$\tilde{\tau} = -\frac{2}{3}\mu_v(\nabla \cdot \vec{u})\tilde{I} + \mu_v[\nabla\vec{u} + (\nabla\vec{u})^T],$$

$$\vec{q} = \mu_e\nabla e.$$

The transport coefficients for momentum and heat fluxes are μ_v and μ_e respectively. In this paper, we restrict our study to laminar flows only. The laminar viscosity is given by the Sutherland law and the Prandtl number is assumed to be a constant value of 0.72 throughout the flowfields.

3. NUMERICAL METHODS

A three-dimensional Chimera grid-embedding technique is incorporated with the full Navier-Stokes code so that the physical domain of the flow field is subdivided into regions which can accommodate easily-generated grids. Extended utilization of such technique is made to do grid adaptation.

Chimera Grid Scheme

The Chimera scheme is a grid embedding technique which provides a conceptually simple method for domain decomposition. For instance, a major grid is usually

4

generated about a main body element and minor grids are then overset on the major grid so as to resolve interesting features of the configuration. Usually, the minor grids are overset on top of the major grid without requiring the mesh boundaries to join in any special way. However, a common or overlap region is always required to provide the means of matching the solutions across boundary interfaces.

To increase the flexibility in the selection of subdomains, the Chimera scheme also allows an implementation to remove regions of a mesh containing an embedded grid from that mesh. That is, an embedded mesh introduces a 'hole' into the mesh in which it is embedded. Typically, a hole is defined through a creation boundary which consists of a surface or a group of surfaces. The purpose of a hole creation boundary is to identify points that are within this boundary. A mesh point is considered to be inside a hole creation boundary if it is inside all surfaces that define the boundary. Figure 1 illustrates the method used to determine whether a point is inside or outside a surface. A mesh point, $\mathbf{P}$, is considered to be inside a surface if the dot product between $\vec{\mathbf{R}}$ (the vector from the closest point on the surface to the mesh point), and $\vec{\mathbf{N}}$ (the normal vector on the surface at the closest point, directed outward from the hole region) is negative or zero. If the dot product is positive, the mesh point is considered to be outside the surface. Because the regions interior to the hole do not enter into the solution process, intergrid communication is simplified since communication among the grids is restricted to the transfer of boundary data. Appropriate boundary values are interpolated from the mesh or meshes in which the boundary is embedded. Communication between overlaid grids is achieved by interpolation of boundary values from grids in which the boundaries are contained. The scheme employs nonconservative tri-linear interpolation that as some simple experiments have shown is superior to Taylor series expansion. The question of conservative vs nonconservative interpolation, is beyond the scope of the present study, and will be a topic of future investigations.

The Chimera procedure naturally separates into two parts, (1) generation of

5

the composite mesh and associated interpolation data and (2) solution of the flow model. The first part has been embodied in a computer code, PEGSUS.[11] PEGSUS takes the independently generated component grids and the embedding structure as input and automatically constructs the composite mesh and interpolation data which are output. More details regarding the embedding grid technique can be found in Ref.[12]

Flow Solver

A computer code based on a time accurate, 3D, finite volume, high resolution scheme for solving the compressible full Navier-Stokes equations has been developed[13]. Based on the finite volume method, equation (1) is semi-discretized by assuming that the cell-centered conserved variables are constant within a cell, and that the flux integral at cell surfaces is also approximated by an average value of the numerical flux and the surface length. The numerical formulation uses a new class of flux splitting schemes[14,15]. The scheme first splits the full flux into convective and pressure fluxes, $\mathbf{F}_{1/2}^{(c)}$ and $\mathbf{F}_{1/2}^{(p)}$ respectively,

$$\mathbf{F}_{1/2} = \mathbf{F}_{1/2}^{(c)} + \mathbf{F}_{1/2}^{(p)} = c_{1/2}\Phi_{L/R} + \mathbf{P}_{1/2} \qquad (3)$$

at the cell interface $L < \frac{1}{2} < R$. The interface pressure, $\mathbf{P}_{1/2}$, simply comprises the "positive" and "negative" data from appropriate domains of dependence via characteristic speed decomposition. The passive scalar variables $\Phi \equiv (\rho, \rho u, \rho H)^T$ is transported by a common convective velocity $u_{1/2}$ that is constructed in a similar fashion as $\mathbf{P}_{1/2}$. Then the upwind idea is used to select the state, i.e., "L" or "R", of the variables to be convected. As such, the interface flux can be recast in the following form:

$$\mathbf{F}_{1/2} = c_{1/2}\frac{1}{2}\Big[\Phi_L + \Phi_R\Big] - \frac{1}{2}|c_{1/2}|\Delta_{1/2}\Phi + \mathbf{P}_{1/2} \qquad (4)$$

where $\Delta_{1/2}(\ ) = (\ )_R - (\ )_L$. Here the first term on the RHS is clearly not a simple average of the "L" and "R" fluxes, but rather a weighted average via the convective

6

velocity.

A variant of the second-order time accurate Lax-Wendroff method is proposed that utilizes identical procedures in both predictor and corrector steps:

$$predictor: \quad \mathbf{U}^* = \mathbf{U}^n + \Delta t \frac{\partial \mathbf{U}^n}{\partial t},$$

$$corrector: \quad \mathbf{U}^{**} = \mathbf{U}^* + \Delta t \frac{\partial \mathbf{U}^*}{\partial t}, \tag{5}$$

$$\mathbf{U}^{n+1} = \frac{1}{2}(\mathbf{U}^n + \mathbf{U}^{**}).$$

As aforementioned, a flow solver must be modified to account for the use of multiple meshes and the "holes" in the grids. These hole points must be blanked or excluded from the flow field solution. The main change in the flow algorithm itself is the treatment of the hole boundaries. The PEGSUS code is used to determine the interpolation coefficients between composite grids. The hole information from the Chimera grid package is stored in an array, IBLANK, which is defined for each point on each grid as

$$\text{IBLANK} = \begin{cases} 1, & \text{if a point is not blanked;} \\ 0, & \text{if a point is blanked.} \end{cases}$$

In the flow solver, each element in the corrector step is multiplied by the appropriate IBLANK value before the solutions are updated:

$$\mathbf{U}^{n+1} = \mathbf{U}^n + \text{IBLANK} \cdot (\mathbf{U}^{n+1} - \mathbf{U}^n) \tag{6}$$

The blanked solutions are updated in the interpolation routine. With this approach, no special routines or logic tests are required to exclude the blanked points from the flow field solution.

Solution-Adaptive Overlaid Meshes

In general, a great flexibility can be found in the procedure by using the overlaid meshes in the region to adapt to the flow with special features. We first obtain a

sufficiently converged solution based on a reasonably coarse grid and then adapt a secondary grid mesh which is clustered and aligned with the solution features such as a shock wave, contact surface, boundary layer, and shear layer. In the shock wave problem, we adapt a fine-mesh system to the shock location without requiring the mesh boundaries to join in any special way. Subsequently, grid points within those high-gradient regions are blanked or excluded from the base grid — i.e. a hole is created on the base (coarse) grid. Communications through boundary interfaces between those separate grids are carried out using tri-linear interpolation. Figure 2 illustrates the connections between composite overlapping grids, with hole points being blanked by a prescribed flow feature such as the shock wave. The idea is that an additional structured grid block is generated to embed on the base grid in high-gradient regions so that the accuracy of the solution will be enhanced.

To be specific, the present methodology provides not only geometrical independence between grid meshes, but also a natural alignment and clustering of grids with features in the solution. In this case, no grids will be sacrificed in the base (coarse) mesh so that the overall accuracy of the flow solutions can be enhanced after the adaptation. Furthermore, the grid orthogonality can be maintained in each grid and the convergence history will not suffer because of grid skewedness. For the test cases shown in this paper, the shock wave is the obvious feature for applying the adaptation procedure. However, in more complex flows, several adaptation criteria may be needed. Determinations in choosing various adaptive criteria, such as the density, pressure, etc., really rely on the users' knowledge. An automatic adaptive grid system is beyond the scope of the present study, and will not be discussed herein.

4. TEST PROBLEMS AND RESULT DISCUSSIONS

The present grid adaptation method has been implemented for inviscid shock

8

reflection, 15° ramp channel flow, laminar flat plate and shock wave/boundary layer interaction problems. The numerical results presented herein show the flexibility of the present method and the accuracy attainable by solution-based enhancement.

Case 1: Inviscid Shock Reflection

We consider a regular reflection of an oblique shock wave from a solid surface. The inflow condition are fully specified with free stream values and the conditions at the top boundary are set to satisfy the shock-jump relations with a specified shock angle. The variables at the outflow boundary are extrapolated linearly. At the solid wall, the slip condition is applied by setting the normal velocity component and the gradient of other variables vanishes.

The first case has an incoming Mach number of 2.9 and a shock angle of 29 degrees. The computational domain containes four independent grid meshes. A base grid of size 59×20 is equally divided in a domain $0.0 \leq x \leq 4.0$, and $0.0 \leq y \leq 1.0$. Additional adapted grids are generated separately to align with the shock location based on a prescribed flow solution. In all cases, it is sufficient that the grid meshes are generated using an algebraic method which uses the edge point information to interpolate grid point values on the surface interior. Figure 3 illustrates the complete composite grid system. As denoted in the figure, GRID1 (59×20) represents the background coarse grid; GRID2 (29×50) and GRID3 (29×50) overset on top of the incoming oblique shock and on the outgoing reflection shock, respectively. The last grid, GRID4 (29×20), resolves the intersection region where the oblique shock impinges against the solid surface.

PEGSUS then composes each grid mesh together and provides the necessary interpolation data before proceeding to the flow solver. As displayed in Fig. 4, the base grids are excluded within the shock region. It is proposed that the shock structure will be resolved by the adapted overlapping grids. The pressure contour for the shock reflection, as illustrated in Figs. 5(a–b), shows an accurate resolving

9

of the shock waves. Figures 6(a–c) plots the comparison of the pressure distribution between numerical calculation and the exact solution along $y=0$. It is noted that numerical results by using the present method predict a sharp transition through the shock waves.

Case 2: 2D Channel with a 15° Ramp

In this case, the steady-state flow is computed in a 2D channel with a 15° ramp. The free-stream Mach number is $M_\infty=1.8$. There is an attached shock at the compression ramp corner, which reflects from the top wall, forming a Mach stem. The Mach number is chosen so that the extent of the Mach stem is about 20% of the channel height. The shock wave continues to reflect from the bottom and top walls, before exiting the channel. The ramp-shoulder expansion fan acts to weaken the first reflected shock. It is noted that a slip line emanates from the triple point at the Mach stem.

Numerical studies are performed based on three different types of grid system. The calculation is first carried out on a single uniform grid of size 69×30 for a domain ($0 \le x \le 3$ and $0 \le y \le 1$), as shown in Fig. 7(a). Figures 7(b) and 7(c) plot the converged results of the flowfield in the form of pressure and Mach contours, respectively. The slip line emanating from the triple point is hardly observed, as shown in Fig. 7(c). Note that the shock wave structures are not well resolved, suggesting a solution improvement is needed there.

By scanning the maximum pressure gradient points from the base grid solution, we adapt four additional meshes which are clustered and aligned with the shock waves. Figure 8(a) shows the connections of the composite grid system. The blanked regions indicating the hole locations on the base grid are displayed in Fig. 8(b). In Figs. 8(c–d) both pressure and Mach contours give an overall qualitative picture of the flow, demonstrating a sharp resolution of the ramp shock, mach stem, and the subsequent shocks. It is worth noting the clear slip line emanating from the triple

point. In sight of those contour plots, the ramp shock is clearly captured and the shock angle is about 51 degrees. In addition, the subsequent shocks are also well resolved.

To validate the above adapted solutions, numerical results are further obtained using a single fine mesh (149×80), as shown in Fig. 9(a). Illustrated in Figs. 9(b) and 9(c) are the computed pressure and Mach contours, respectively. The detailed quantitative profiles along the lower and upper solid boundaries are compared among the present results and various single mesh solutions, as displayed in Figs. 10(a–d) and 11(a–d). It is evident that the solution-adaptive overlapping meshes enhance an accurate prediction for the ramp shock and subsequent shock locations along the lower surface in Figs. 10(a–d). No attempt has been made to adapt the ramp-shoulder expansion fan, so that the fan is slightly smeared due to the coarse grid structure. For the upper surface, Figs. 11(a–d) show that the shock locations are also accurately predicted when the present method is applied. Also observed in the coarse grid solution, an early reflecting shock position is predicted. In general, we show that the coarse grid system has the difficulty in predicting the correct locations for oblique shock, mach stem, and the subsequent shock waves. However, by using the overlapping adaptive meshes, we are capable of capturing accurately the shock structures and other salient features.

Case 3: Flat Plate Boundary Layer Flow

A compressible, laminar flat plate flow problem is computed to validate the implementation of Chimera overset meshes for viscous flow. Figure 12 illustrates the solution-adaptive grid system used in the computational domain. It contains two independent grid meshes with an overlapping region being used to connect the grid boundaries. The spacing of GRID1 is refined using a hyperbolic-tangent stretching function in the streamwise direction in the vicinity of the leading-edge, followed by increasing cell spacing downstream. The second grid system, GRID2,

extends downstream using an equal-spacing distribution in the streamwise direction. A hyperbolic-tangent stretching function is applied to stretch the grid in the normal direction in both meshes.

Boundary conditions include a Mach 2 freestream inflow, exit outflow extrapolation, and outflow extrapolation at the top boundary to avoid artificially constraining the normal velocity component. An invicid wall is assumed forward of the plate leading-edge. Laminar flow upstream of the leading edge starts to develop a boundary layer at the leading edge. A no-slip condition is applied on the adiabatic flat plate.

To validate our numerical results, comparisons are made between the present numerical results and that obtained by solving the boundary-layer equations. The boundary-layer equation for a flat plate in the absence of pressure gradient is derived using the Mangler-Levy-Lees transformations

$$d\zeta = \rho_e \mu_e u_e dx \qquad (7a)$$

$$d\eta = [\rho_e u_e / (2\zeta)^{1/2}](\rho/\rho_e)dy \qquad (7b)$$

where the subscript e denotes the fluid properties at the edge of boundary layer. x is the distance along the body, and y normal to it. In ζ-η coordinates, the boundary-layer equations are written as[16]

$$(cf'')' + ff'' = 0 \qquad (8a)$$

$$(a_1 g' + a_2 f' f'')' + fg' = 0 \qquad (8b)$$

in which

$$f' = u/u_e, \qquad g = h/h_e, \qquad c = \rho\mu/\rho_e\mu_e,$$

$$a_1 = c/Pr, \qquad a_2 = \frac{(\gamma-1)M_e^2}{1 + \left(\frac{\gamma-1}{2}\right)M_e^2}\left(1 - \frac{1}{Pr}\right)c$$

12

where the superscript prime denotes partial differentiation with respect to η. Here h is the enthalpy and M_e is the edge Mach number. The normal velocity component is then obtained by solving the continuity equation:

$$\frac{\partial(\rho u)}{\partial x} + \frac{\partial(\rho v)}{\partial y} = 0. \tag{9}$$

The numerical solutions of the present method, as shown in Fig. 13, illustrate self-similar profiles of the streamwise velocity distributions at various downstream locations (i=30 of GRID1, i=15 and 38 of GRID2). Note that the profiles are plotted against a transformed coordinate $\eta = y\sqrt{u_\infty / \nu_\infty x}$. This mainly shows that the fluid fluxes are accurately transferred through the interfaces of grid boundaries. It is also found that such similarity extends to the normal velocity distributions and to the temperature fields. Figure 14(a) compares the streamwise velocity component between the present numerical result and the boundary-layer solution (Eqs. 8a–b) at a downstream location (i=47 of GRID2) behind the grid interfaces. The normal velocity distributions and the temperature profiles are also compared respectively in Figs. 14(b) and 14(c). It is evident that the present method obtains a very good agreement with the boundary-layer solution, indicating that the accuracy of the numerical results using overlapping meshes is well preserved.

Case 4: Shock Wave/Boundary Layer Interaction

The current method is readily applied to the shock wave/boundary layer interaction problem. The experiment by Hakkinnen et al.[17] at M_∞=2.0, Re_∞=2.96×10^5 and shock angle=32.585° was chosen for calculation using the adapted overlapping grids. The flow is observed that the leading-edge shock wave induced by the start of the boundary layer becomes noticeably weaker after intersecting with an impinging oblique shock wave. The oblique shock is sufficiently strong to induce a sizable separation, which in turn causes the formation of the 'separation shock' as the mainstream encounters a change of effective 'body'. An expansion fan is created

as the streamline changes the slope, roughly at the pressure 'plateau'. Finally the 'reattachment shock' wave is developed corresponding to further rise of the pressure.

A single fine mesh using 100 by 120 in the streamwise and normal directions, respectively, is first chosen to simulate the Mach 2 flow. As displayed in Fig. 15, grid spacing in the normal direction is stretched near the solid boundary which allows a better resolution of the boumdary layer. The resulting pressure contours are plotted in Fig. 16. Enhancement of the flow solution is then performed using overlapping adaptive meshes. Figure 17 illustrates the solution-adaptive grid system which contains three independent meshes: GRID1 (100×80) resolves the boundary layer region; GRID2 (80×40) covers the flowfield beyond the boundary layer; and GRID3 (30×20) catches the incoming oblique shock wave. It is observed that the present method obtains a significant improvement to the flowfield and, in particular, to those shock structures, as shown in Fig. 18. We further compare the pressure ratio and skin friction along the flat plate with those by Hakkinnen et al.[17] While many other calculations have been reported, the reattachment point in general is much harder to predict accurately than the separation point. Figure 19 displays a very good agreement of the enhanced solution with the experimental data in the surface pressure ratio at both separation and reattachment points. However, the skin friction in Fig. 20 shows a slight discrepancy in the separation region.

5. CONCLUDING REMARKS

We have presented a solution-adaptive enhancement method using Chimera composite overlapping meshes and shown its capability for crisply capturing high-gradient regions. Applications to various shock reflection and shock wave/boundary layer interaction problems are tested. The successful implementation of the Chimera overset grid in combination with a Navier-Stokes solver serves as a useful tool that enhances the accuracy of salient features of the flowfield, such as shock and reflection

14

waves. Unlike other grid adaptation methods, the present methodology would not create high aspect-ratio or highly skewed cells in the grid system so that a reduced convergence rate is avoided. The strategy from Chimera overset grid also provides a great flexibility in grid generation for complex configurations.

ACKNOWLEDGEMENTS

References

[1]Benek, J. A., Buning, P. G. and Steger, J. L., "A 3-D Chimera Grid Embedding Technique," AIAA Paper 85-1523, 1985.

[2]Gnoffo, P. A., "A Vectorized, Finite Volume, Adaptive Grid Algorithm for Navier-Stokes," *Numerical Grid Generation*, Editor: Thompson, J. F., North-Holland, NY, 1982, pp. 819–836.

[3]Brackbill, J. U., "Coordinate System Control: Apadtive Meshes," *Numerical Grid Generation*, Editor: Thompson, J. F., North-Holland, NY, 1982, pp. 277–294.

[4]Saltzman, J. and Brackbill, J. U., "Applications and Generalizations of Variational Methods for Generating Adaptive Systems," *Numerical Grid Generation*, Editor: Thompson, J. F., North-Holland, NY, 1982, pp. 865–884.

[5]Berger, M. J., "Adaptive Mesh Refinement for Hyperbolic Partial Differential Equations," STAN-CS-82-924, Standford University, August 1982.

[6]Eiseman, P. R., "Adaptive Grid Generation by Mean Value Relaxation," *Advances in Grid Generation*, Editors: Ghia, K. N. and Ghia, U., ASME-FED-5, 1983, pp. 29-34. (Also in ASME J. Fluids Engrg., Vol. 107, 1985, pp. 477–483).

[7]Eiseman, P. R., "Adaptive Grid Generation," *Computer Methods in Applied Mechanics and Engineering*, Vol. 64, North-Holland, 1987, pp. 321–376.

[8]Nakahashi, K. and Diewert, G. S., "A Three-Dimensional Adaptive Grid Method," AIAA Paper 85-0486, 1985.

[9]Gonnett, W. C., Agarwal, R. K. and Schwartz, A. L., "An Adaptive Grid-Generation Scheme for Flowfield Calculations," AIAA Paper 87-0199, 1987.

[10]Gonnett, W. C., Agarwal, R. K. and Schwartz, A. L., "An Adaptive Grid-Algorithm for the Euler/Navier-Stokes Equations," AIAA Paper 88-0519, 1988.

[11]Suhs, N. E. and Tramel, R. W., "PEGSUS 4.0 User's Manual," AEDC-TR-91-8, November 1991.

[12]Benek, J. A., Steger, J. L., Dougherty, F. C. and Buning, P. G., "Chimera: A Grid-Embedding Technique," AEDC-TR-85-64, April 1986.

[13]Liou, M. S. and Hsu, A. T., "A Time Accutate Finite Volume High Resolution Scheme for Three Dimensional Navier-Stokes Equations," AIAA Paper 89-1994-CP, 1989.

[14]Liou, M. S. and Steffen, C. J. Jr., "A New Flux Splitting Scheme," NASA-TM-104404, May 1991.

[15]Liou, M. S., "On A New Class of Flux Splittings," 13th International Conference on Numerical Methods for Fluid Dynamics, Rome, Italy, July 1992.

[16]Cebeci, T. and Smith, A. M. O., *Analysis of Turbulent Boundary Layers*, Academic Press, New York, 1974.

[17]Hakkinen, R. J., Greber, I., Trilling, L. and Abarbanel, S. S., "The Interaction of an Oblique Shock Wave with a Laminar Boundary Layer," NASA MEMO 2-18-59W, 1959.
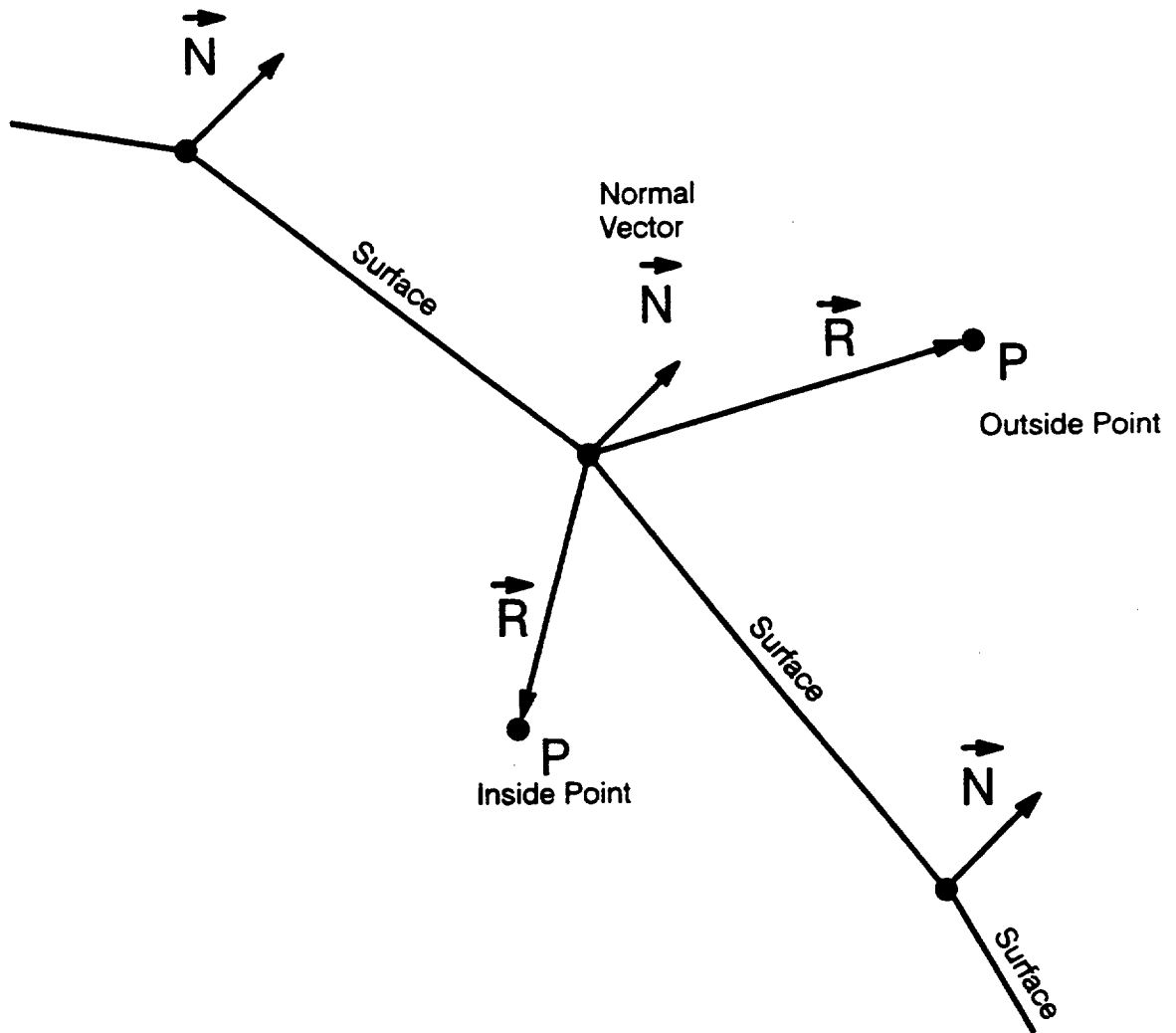
Fig. 1 Mesh point considered to be inside or outside a surface.
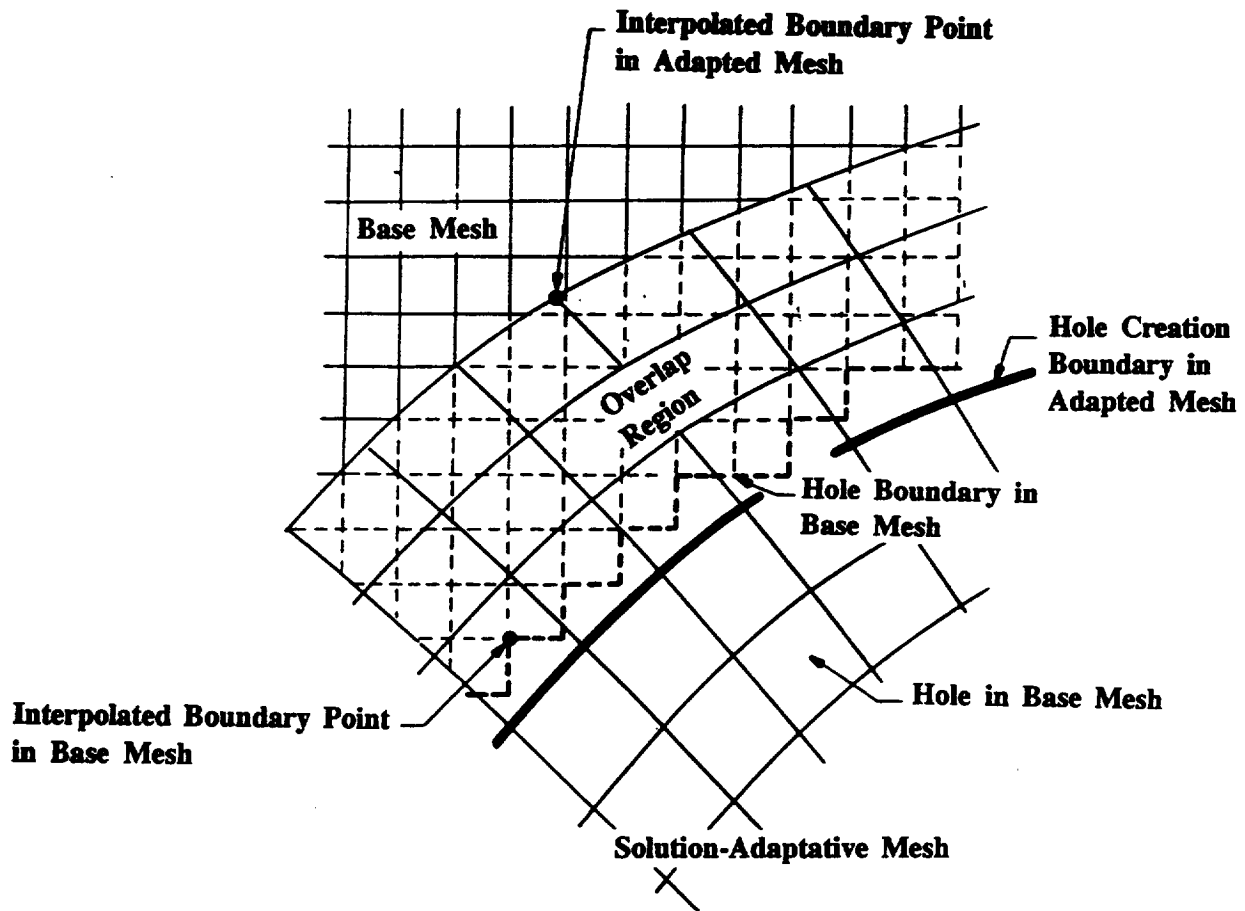
Fig. 2 Overset grids for base mesh and solution-adaptative mesh.
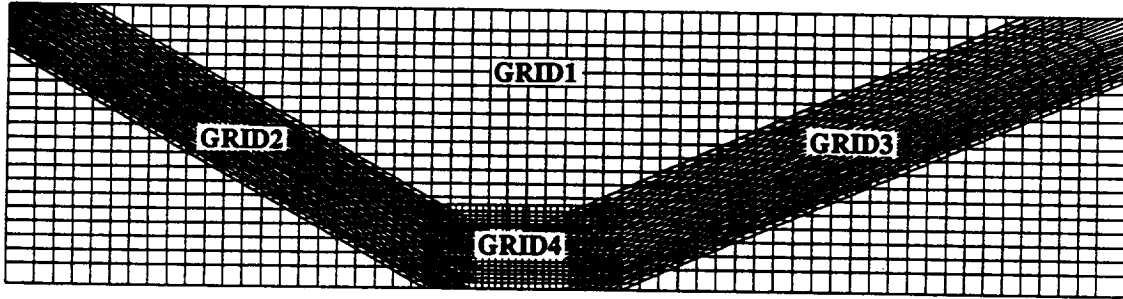
Fig. 3 Composite overlapping grid system for inviscid shock reflection problem;
GRID1 (59×20), GRID2 (29×50), GRID3 (29×50), GRID4 (29×20).
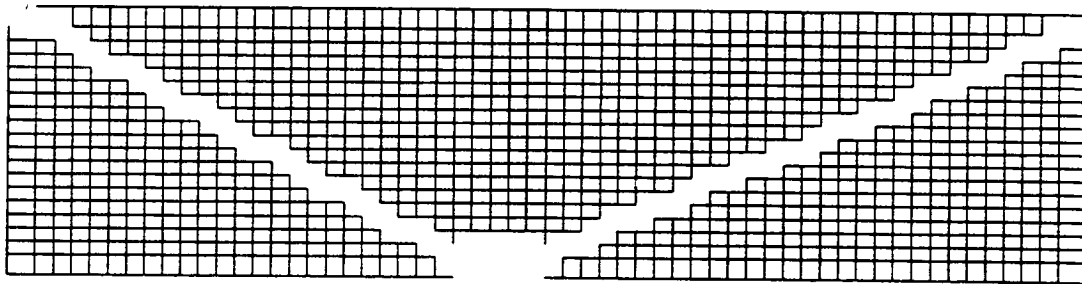
**Fig. 4** Background mesh (GRID1) with 'hole' grids blanked in high-gradient regions.
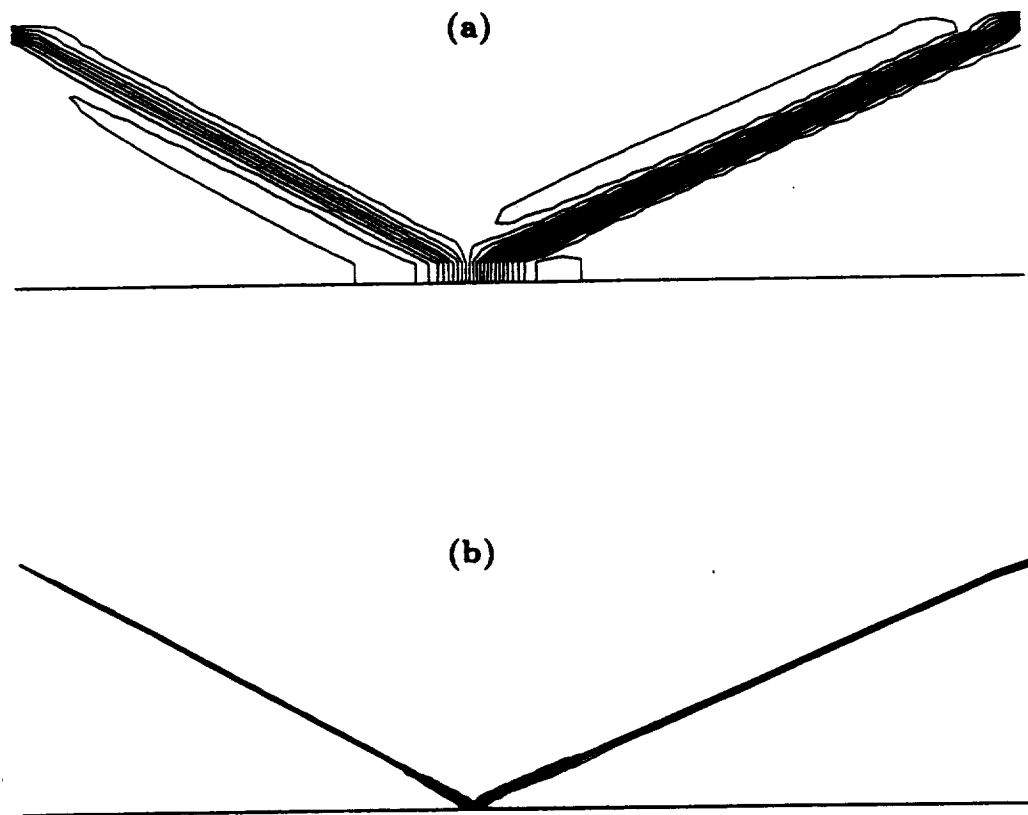
Fig. 5 Pressure contours for shock reflection problem. (a)single grid 59×20, (b)overlapping grids. ($M_\infty = 2.9$, shock angle = 29°, $p_{min} = 0.6$, $p_{max} = 4.0$, $\Delta p = 0.1$)
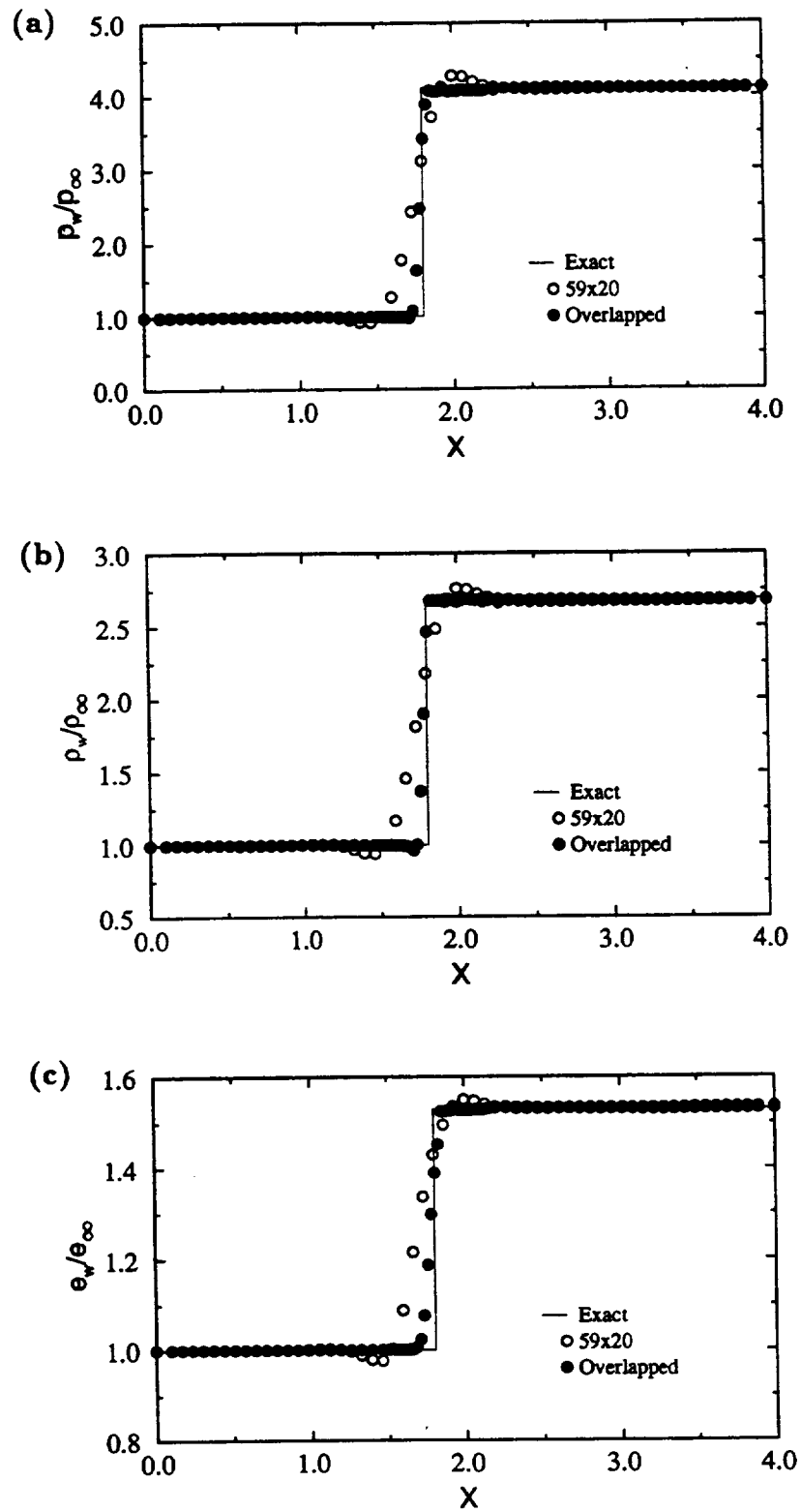
Fig. 6 Variable profiles along solid surface ($y=0$) for inviscid shock reflection problem. (a)pressure, (b)density, (c)internal energy.

21
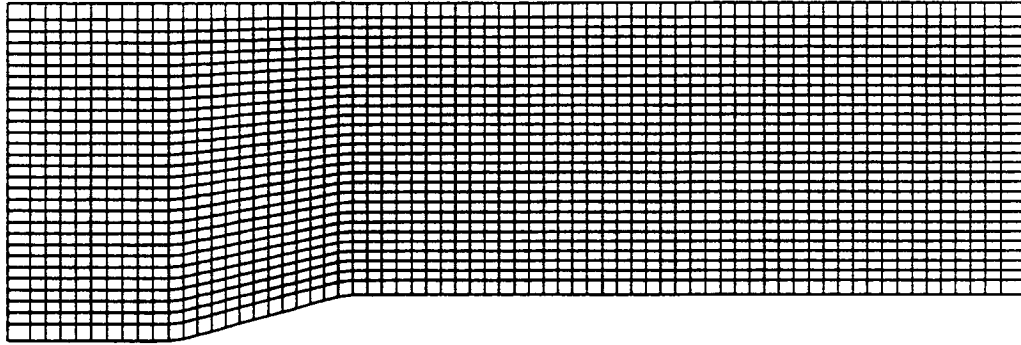
Fig. 7(a) Single coarse grid (69×30) for a 15° ramp channel flow.
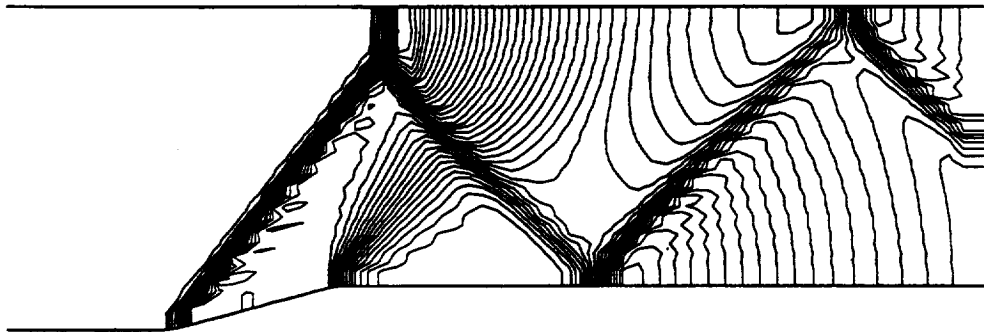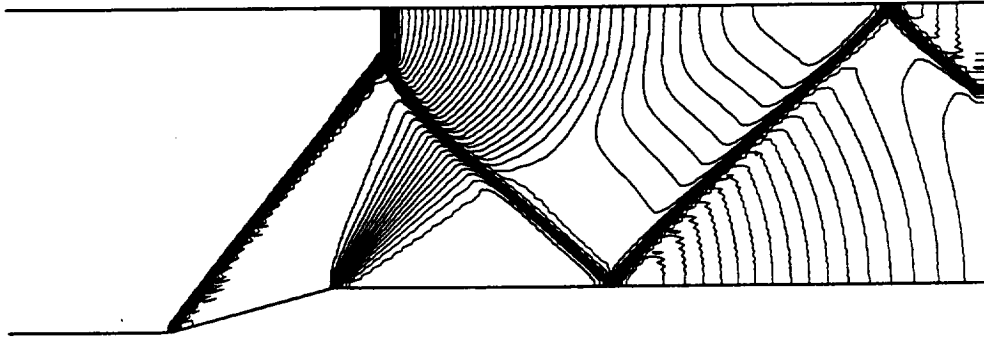

Fig. 7(b) Pressure contours for a 15° ramp channel flow. (69×30)
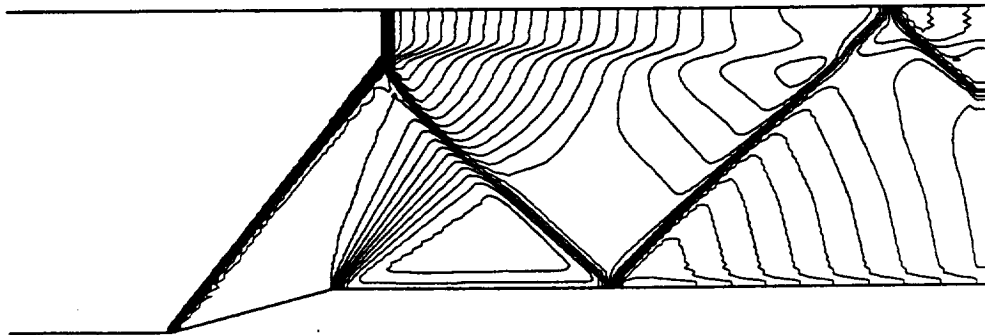($M_\infty = 1.8$, $p_{min} = 0.7$, $p_{max} = 2.7$, $\Delta p = 0.05$)
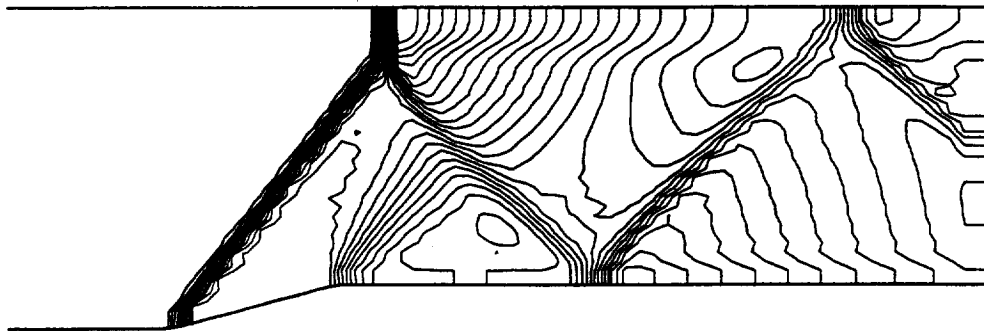
Fig. 7(c) Mach contours for a M_∞=1.8 inviscid flow in a channel with a 15° ramp.
($M_{min} = 0.6$, $M_{max} = 1.8$, $\Delta M = 0.05$, 69×30)

22
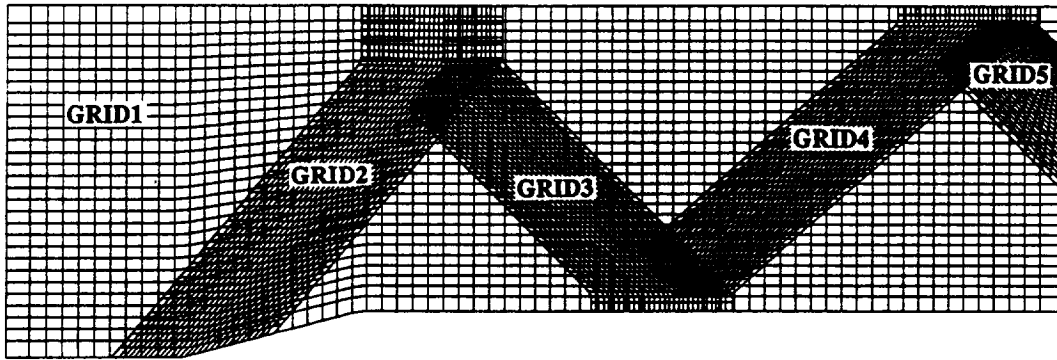
Fig. 8(a)   Composite overlapping grid system for a 15° ramp channel flow;
GRID1 (69×30), GRID2 (29×50), GRID3 (29×50), GRID4 (29× 50),
GRID5 (29×20).
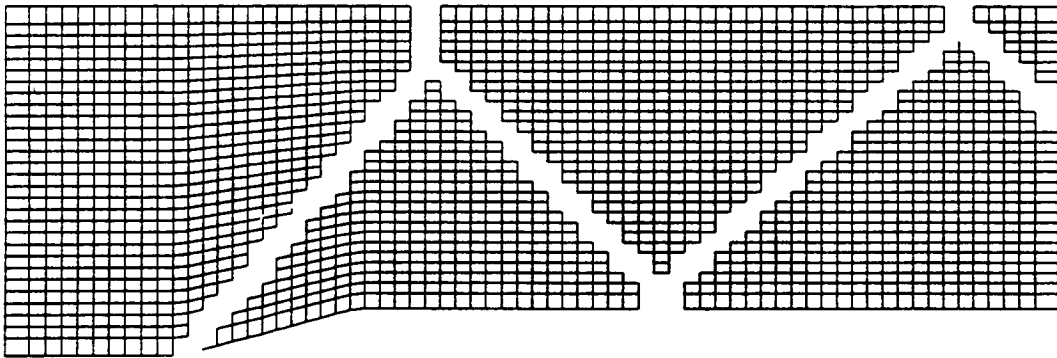
Fig. 8(b)   Base grid (GRID1) with 'hole' grids blanked in high-gradient regions.
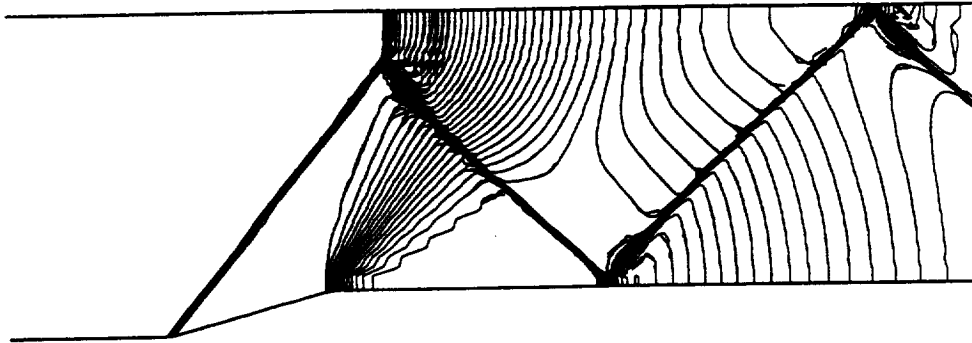
Fig. 8(c) Pressure contours for a 15° ramp channel flow with composite adaptive meshes. ($M_\infty = 1.8$, $p_{min} = 0.7$, $p_{max} = 2.7$, $\Delta p = 0.05$)
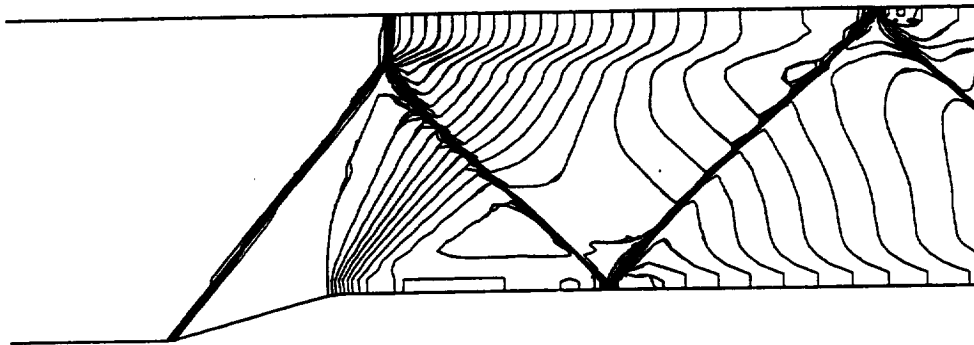
Fig. 8(d) Mach contours for a $M_\infty = 1.8$ inviscid flow in a channel with a 15° ramp. ($M_{min} = 0.6$, $M_{max} = 1.8$, $\Delta M = 0.05$, adapted overlapping meshes)

24
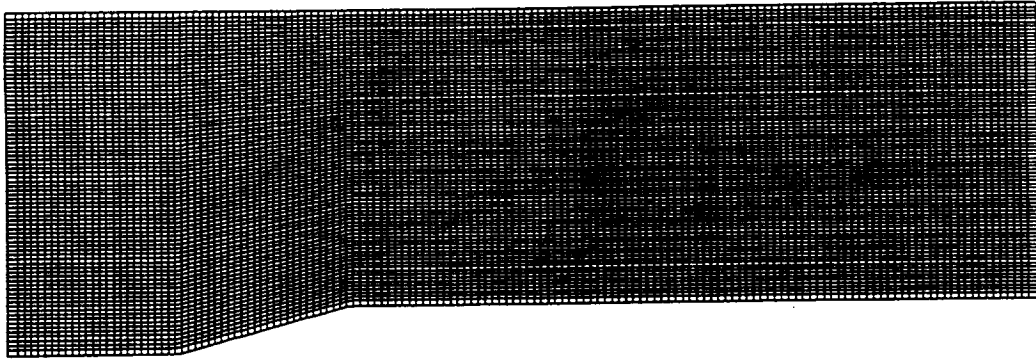
Fig. 9(a) Fine grid mesh (149×80) for a 15° ramp channel flow.

Fig. 9(b) Pressure contours for a 15° ramp channel flow. (149×80)
($M_\infty = 1.8$, $p_{min} = 0.7$, $p_{max} = 2.7$, $\Delta p = 0.05$)

Fig. 9(c) Mach contours for a M_∞=1.8 inviscid flow in a channel with a 15° ramp.
($M_{min} = 0.6$, $M_{max} = 1.8$, $\Delta M = 0.05$, 149×80)

25
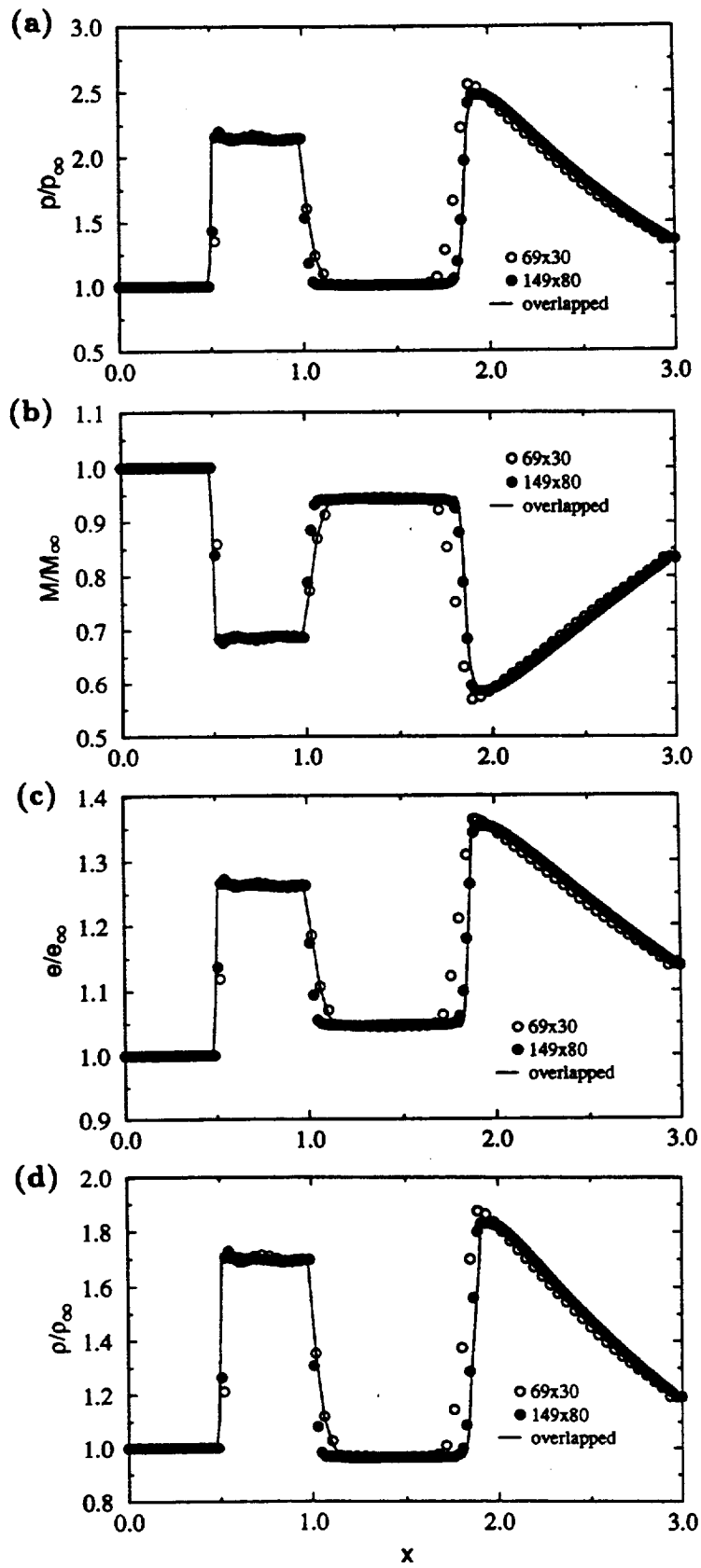
Fig. 10 Variable profiles along the lower solid wall.
(a)pressure, (b)Mach number, (c)internal energy, (d)density.
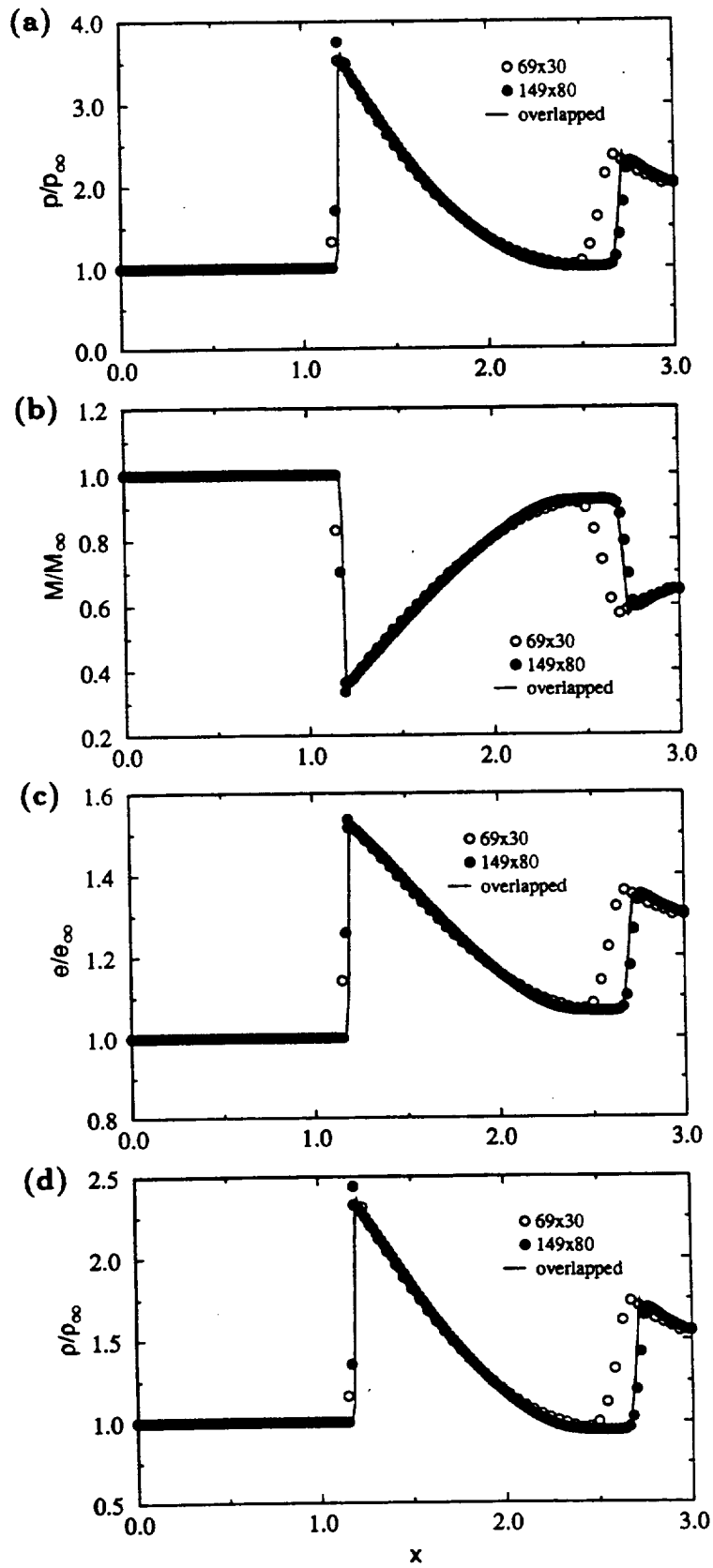
Fig. 11 Variable profiles along the upper solid wall.
(a)pressure, (b)Mach number, (c)internal energy, (d)density.
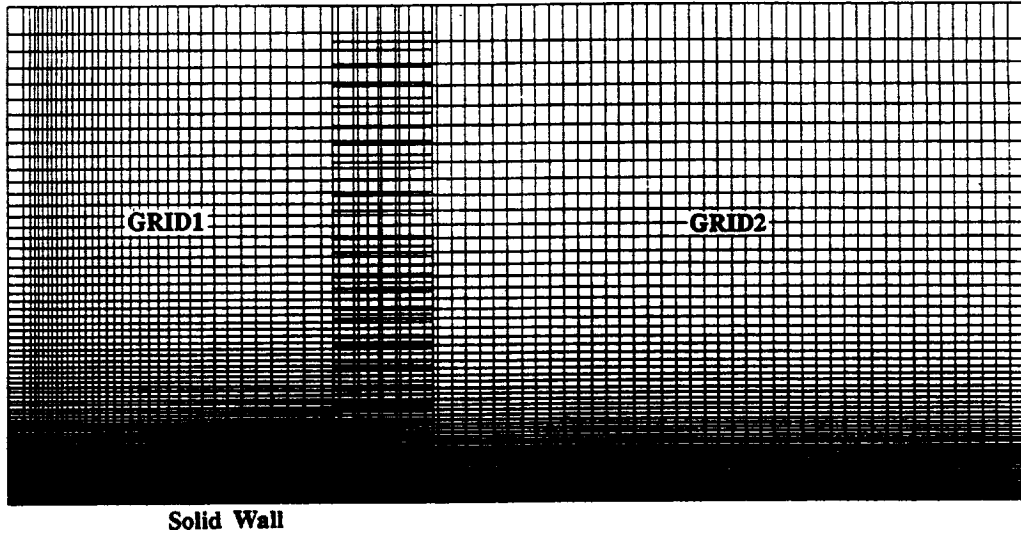
Fig. 12 Composite grid system for laminar flat plate problem; GRID1 (40×100), GRID2 (50×80).
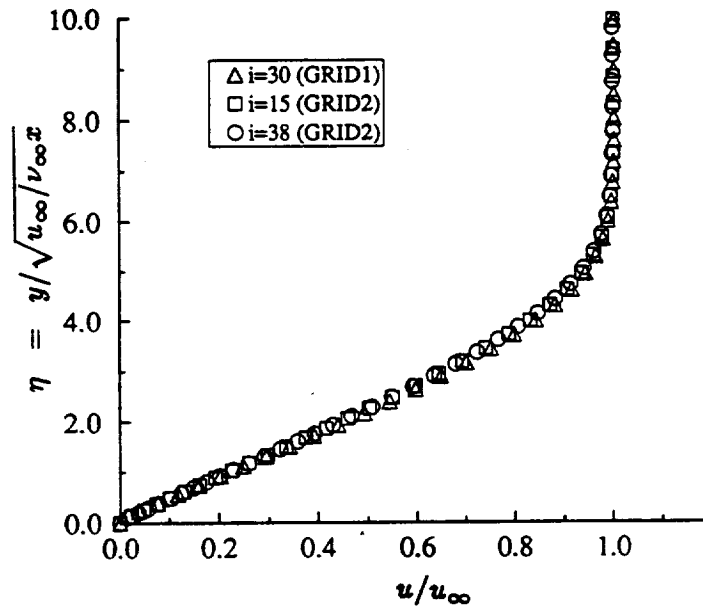

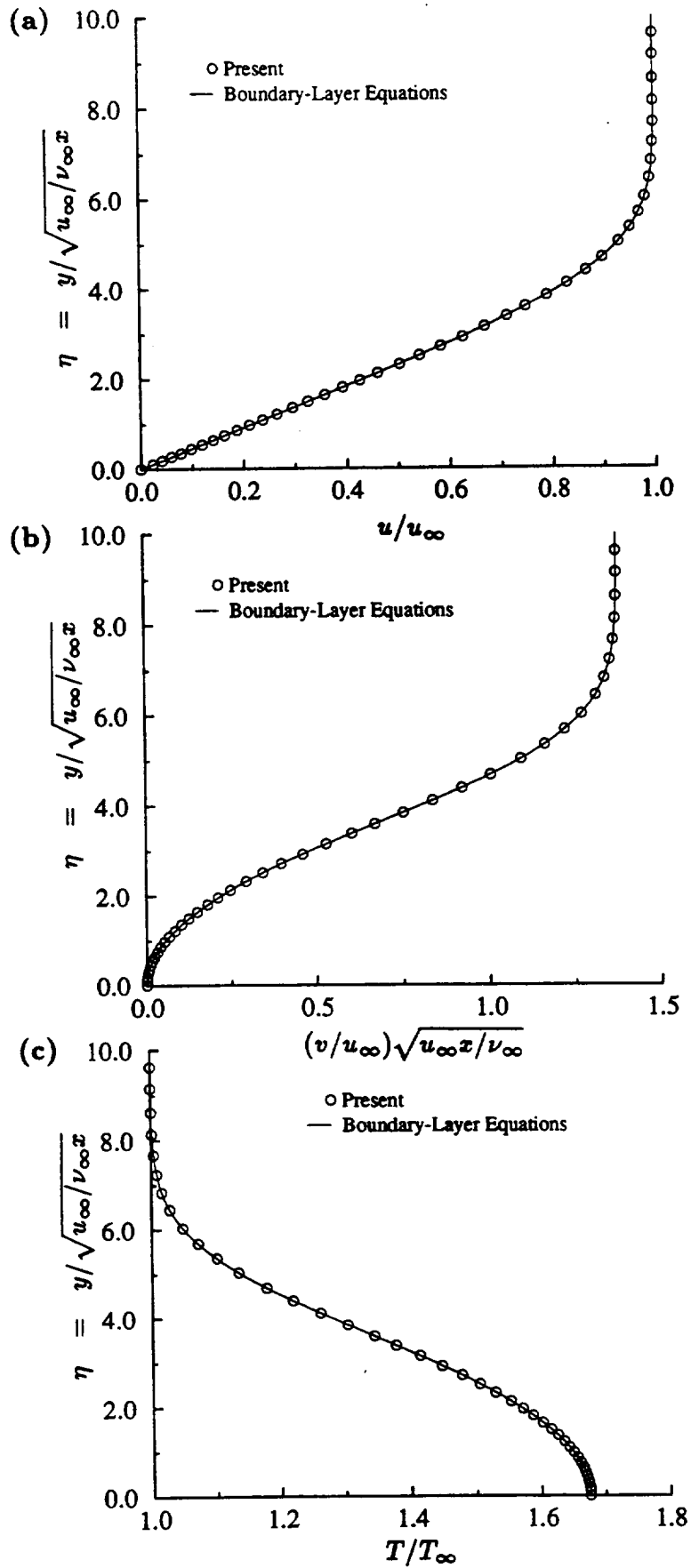**Fig. 13** Self-similar profiles of the streamwise velocity distribution at various down-stream locations. M_∞=2.

Fig. 14 Comparisons of velocity and temperature distributions at a downstream location. (a)streamwise velocity, (b)normal velocity, (c)temperature.
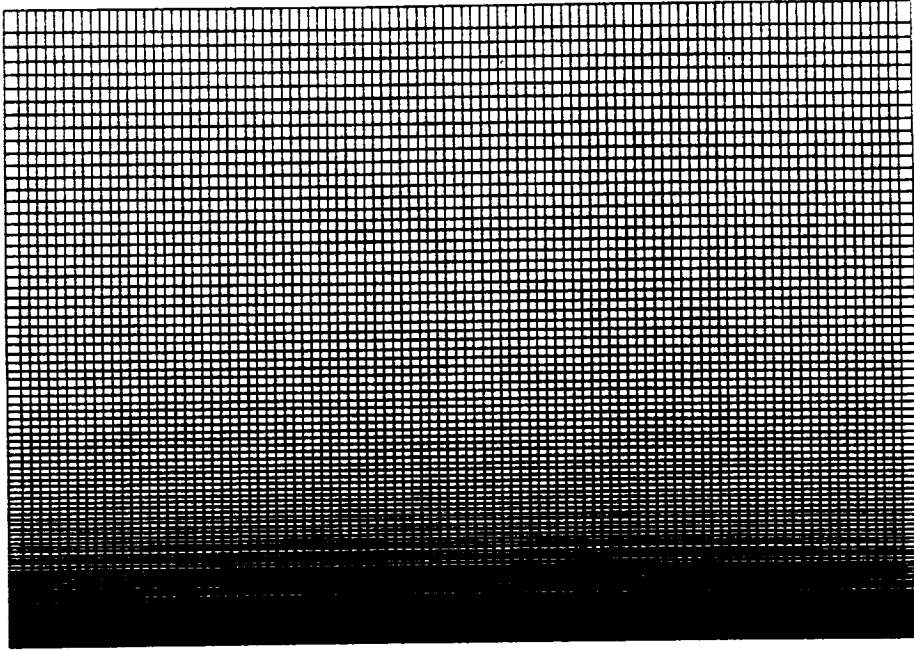
Fig. 15 Single fine grid system for the shock wave/boundary layer interaction. (100×120)
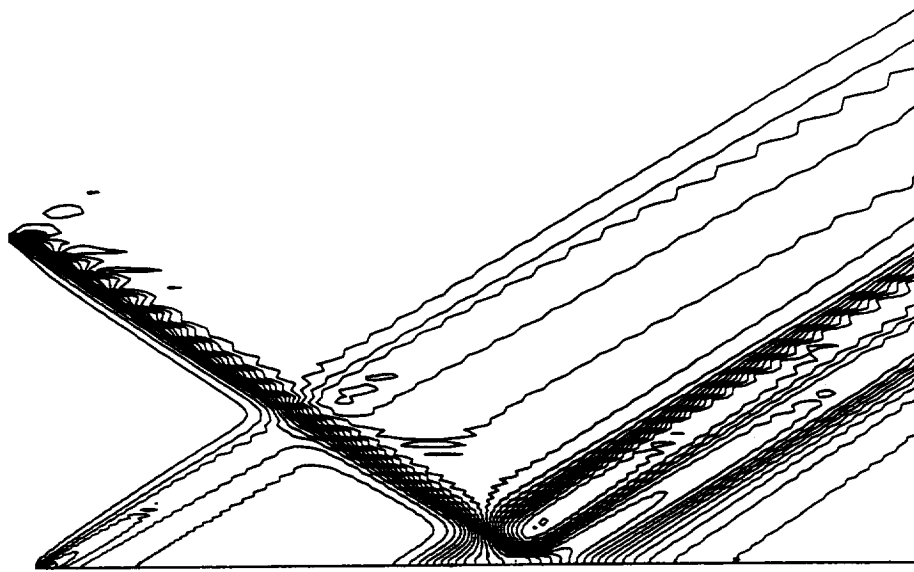

Fig. 16 Pressure contours for shock wave/boundary layer interaction problem with $M_\infty=2.0$, $Re_\infty=2.96\times10^5$, and shock angle = 32.585°. ($p_{min}=0.7$, $p_{max}=1.1$, $\Delta p=0.01$)
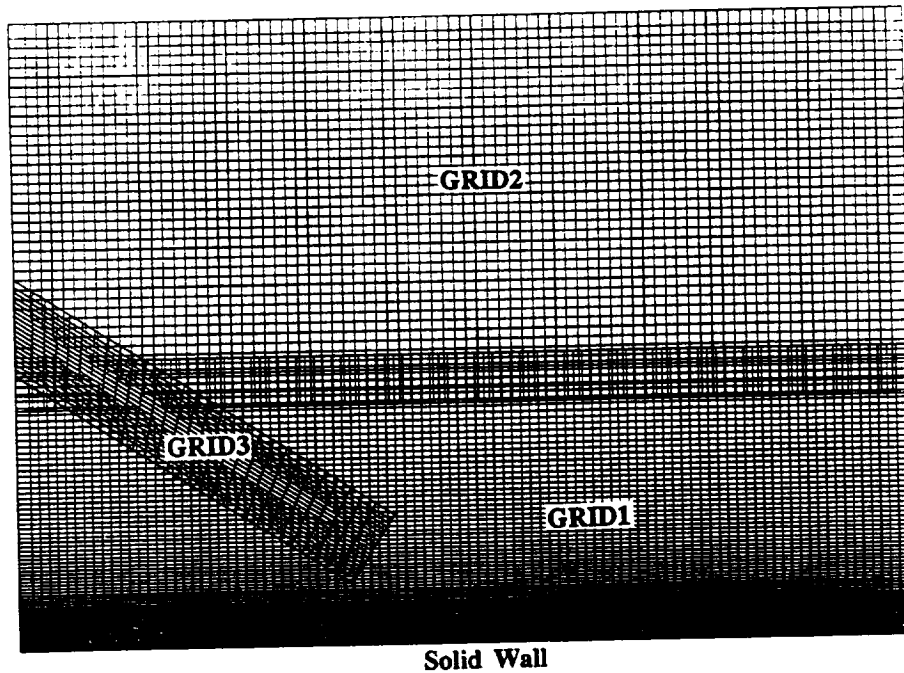
Fig. 17 Composite grid system for shock wave/boundary layer interaction problem; GRID1 (100×80), GRID2 (80×40), GRID3 (30×20).
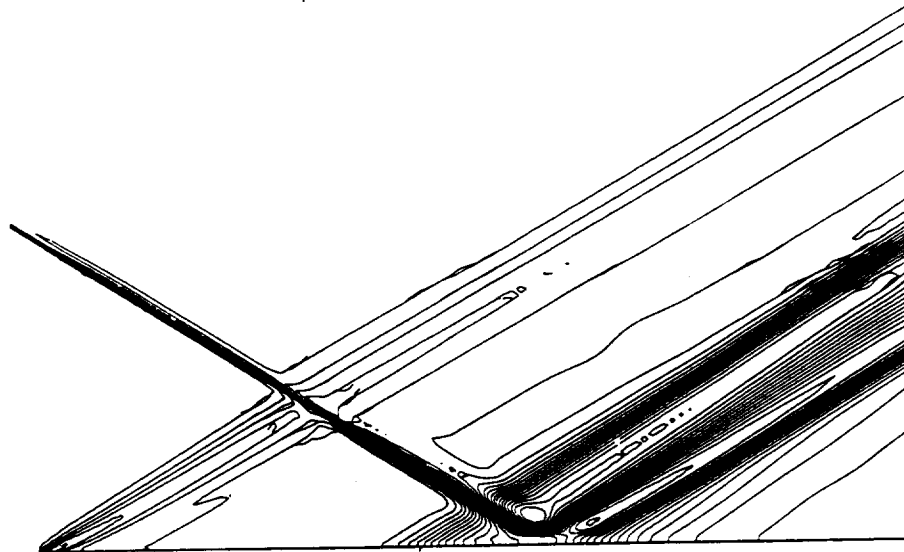

Fig. 18 Pressure contours for shock wave/boundary layer interaction with composite adaptive meshes. ($M_\infty=2.0$, $Re_\infty=2.96\times10^5$, shock angle = 32.585°, $p_{min}=0.7$, $p_{max}=1.1$, $\Delta p=0.01$)
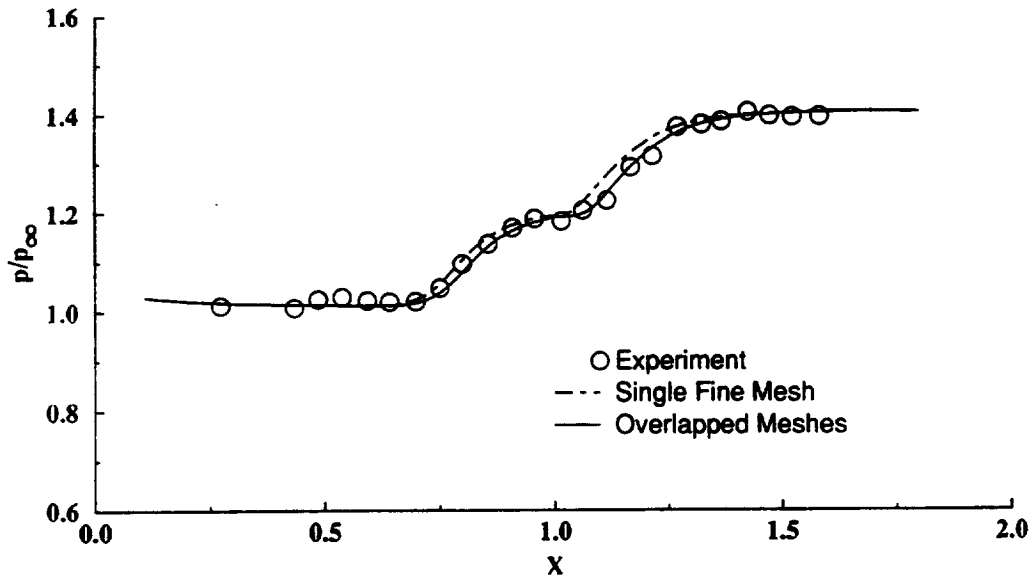
31

Fig. 19 Comparison of surface pressure ratio for shock wave/boundary layer interaction. (M_∞=2.0, Re_∞=2.96×10⁵)
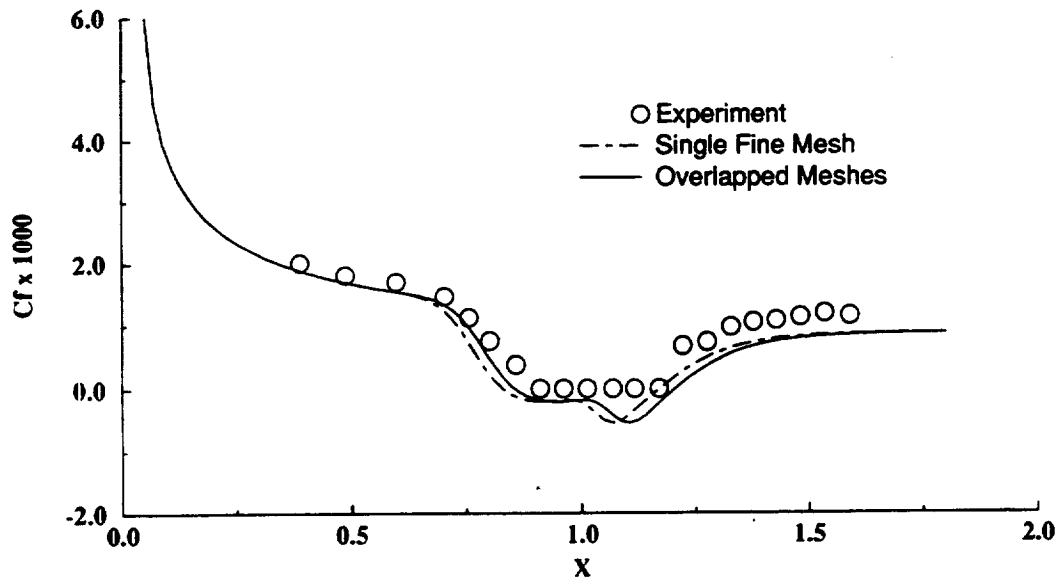

Fig. 20 Comparison of skin friction coefficient for shock wave/boundary layer interaction. (M_∞=2.0, Re_∞=2.96×10⁵)

REPORT DOCUMENTATION PAGE

Public reporting burden for this collection of information is estimated to average 1 hour per response, including the time for reviewing instructions, searching existing data sources, gathering and maintaining the data needed, and completing and reviewing the collection of information. Send comments regarding this burden estimate or any other aspect of this collection of information, including suggestions for reducing this burden, to Washington Headquarters Services, Directorate for Information Operations and Reports, 1215 Jefferson Davis Highway, Suite 1204, Arlington, VA 22202-4302, and to the Office of Management and Budget, Paperwork Reduction Project (0704-0188), Washington, DC 20503.

1. AGENCY USE ONLY (Leave blank)	2. REPORT DATE	3. REPORT TYPE AND DATES COVERED
	May 1993	Technical Memorandum

4. TITLE AND SUBTITLE

Grid Adaptation Using Chimera Composite Overlapping Meshes

5. FUNDING NUMBERS

WU-505-90-5X

6. AUTHOR(S)

Kai-Hsiung Kao, Meng-Sing Liou, and Chuen-Yen Chow

7. PERFORMING ORGANIZATION NAME(S) AND ADDRESS(ES)

National Aeronautics and Space Administration
Lewis Research Center
Cleveland, Ohio 44135-3191

8. PERFORMING ORGANIZATION REPORT NUMBER

E-7855

9. SPONSORING/MONITORING AGENCY NAME(S) AND ADDRESS(ES)

National Aeronautics and Space Administration
Washington, D.C. 20546-0001

10. SPONSORING/MONITORING AGENCY REPORT NUMBER

NASA TM-106163
AIAA-93-3389
ICOMP-93-16

11. SUPPLEMENTARY NOTES

Prepared for the AIAA 11th Computational Fluid Dynamics Conference, Orlando, Florida, July 6-9, 1993. Kai-Hsiung Kao, Institute for Computational Mechanics in Propulsion, NASA Lewis Research Center, (work funded under NASA Cooperative Agreement NCC3-233). Meng-Sing Liou, NASA Lewis Research Center; and Chuen-Yen Chow, Department of Aerospace Engineering Sciences, University of Colorado, Boulder, Colorado 80309. ICOMP Program Director, Louis A. Povinelli, (216) 433-5818

12a. DISTRIBUTION/AVAILABILITY STATEMENT

Unclassified - Unlimited
Subject Category 64

12b. DISTRIBUTION CODE

13. ABSTRACT (Maximum 200 words)

The objective of this paper is to perform grid adaptation using composite over-lapping meshes in regions of large gradient to capture the salient features accurately during computation. The Chimera grid scheme[1], a multiple overset mesh technique, is used in combination with a Navier-Stokes solver. The numerical solution is first converged to a steady state based on an initial coarse mesh. Solution-adaptive enhancement is then performed by using a secondary fine grid system which oversets on top of the base grid in the high-gradient region, but without requiring the mesh boundaries to join in any special way. Communications through boundary interfaces between those separated grids are carried out using tri-linear interpolation. Applications to the Euler equations for shock reflections and to a shock wave/boundary layer interaction problem are tested. With the present method, the salient features are well resolved.

14. SUBJECT TERMS

Grid adaptation; Chimera overset grid; Navier-Stokes equations; Shock waves

15. NUMBER OF PAGES

34

16. PRICE CODE

A03

17. SECURITY CLASSIFICATION OF REPORT	18. SECURITY CLASSIFICATION OF THIS PAGE	19. SECURITY CLASSIFICATION OF ABSTRACT	20. LIMITATION OF ABSTRACT
Unclassified	Unclassified	Unclassified	